Published online 8 February 2014 *Nucleic Acids Research, 2014, Vol. 42, No. 8* ***5217–5233***
doi:10.1093/nar/gku129

The activation of the decapping enzyme DCP2 by DCP1 occurs on the EDC4 scaffold and involves a conserved loop in DCP1

Chung-Te Chang, Natalia Bercovich, Belinda Loh, Stefanie Jonas and Elisa Izaurralde*

Department of Biochemistry, Max Planck Institute for Developmental Biology, Spemannstrasse 35, 72076 Tübingen, Germany

Received October 21, 2013; Revised January 11, 2014; Accepted January 21, 2014

ABSTRACT

The removal of the 5′-cap structure by the decapping enzyme DCP2 and its coactivator DCP1 shuts down translation and exposes the mRNA to 5′-to-3′ exonucleolytic degradation by XRN1. Although yeast DCP1 and DCP2 directly interact, an additional factor, EDC4, promotes DCP1–DCP2 association in metazoan. Here, we elucidate how the human proteins interact to assemble an active decapping complex and how decapped mRNAs are handed over to XRN1. We show that EDC4 serves as a scaffold for complex assembly, providing binding sites for DCP1, DCP2 and XRN1. DCP2 and XRN1 bind simultaneously to the EDC4 C-terminal domain through short linear motifs (SLiMs). Additionally, DCP1 and DCP2 form direct but weak interactions that are facilitated by EDC4. Mutational and functional studies indicate that the docking of DCP1 and DCP2 on the EDC4 scaffold is a critical step for mRNA decapping *in vivo*. They also revealed a crucial role for a conserved asparagine–arginine containing loop (the NR-loop) in the DCP1 EVH1 domain in DCP2 activation. Our data indicate that DCP2 activation by DCP1 occurs preferentially on the EDC4 scaffold, which may serve to couple DCP2 activation by DCP1 with 5′-to-3′ mRNA degradation by XRN1 in human cells.

INTRODUCTION

The removal of the mRNA 5′-cap structure by DCP2 is a critical step in both bulk mRNA turnover and in specific mRNA decay pathways triggered by the presence of AU-rich elements, a nonsense codon or miRNA-binding sites (1). Decapping inhibits translation initiation and commits the mRNA to full degradation by the 5′-to-3′ exonuclease XRN1 (1–3). Although DCP2 is catalytically active *in vitro* (4–7), its activity is stimulated by additional proteins termed decapping activators or enhancers of decapping (1–3). In metazoan, these proteins include DCP1, EDC3, EDC4 (also known as Hedls or Ge-1), RAP55 (also known as LSm14A), Pat, the LSm1–7 complex and the RNA helicase RCK (also known as DDX6/p54) (1,3). These activators may facilitate decapping directly or indirectly by inhibiting translation and/or promoting mRNP rearrangements that expose the cap structure for cleavage by DCP2 (1,3).

DCP2 belongs to the Nudix family of pyrophosphatases and catalyzes the hydrolysis of the cap structure, releasing m^7GDP and a 5′ monophosphorylated mRNA (4–7). DCP2 orthologs feature a catalytic Nudix domain flanked on the N-terminus by an α-helical regulatory domain (NRD) and on the C-terminus by a highly divergent extension (Figure 1A) (4,5,8–10). The NRD of yeast Dcp2 interacts directly with Dcp1 and is required for decapping both *in vivo* and *in vitro* (10,11).

Structural studies of the *Schizosaccharomyces pombe* (*Sp*) Dcp2 revealed that the NRD and the Nudix domain are connected by a flexible hinge region and can adopt multiple conformations relative to each other. These conformations can be classified as open or closed and represent transition states between inactive and active catalysis (3,10,12–14). In the open conformation, the two domains are far apart, and the active site is incomplete. In the closed conformation, the NRD and the Nudix domains interact, forming a composite active site. Dcp2 closure is promoted by cap analogs and Dcp1, leading to the model that Dcp1 enhances decapping by binding to the NRD and stabilizing the closed Dcp2 conformation (1–3,10,12–14). However, how this is achieved in molecular terms remains unresolved (14).

Surprisingly, the DCP1 residues involved in DCP2 binding are not well conserved (10). Accordingly, it has been suggested that human DCP1 and DCP2 do not interact directly, and an additional, metazoan-specific

*To whom correspondence should be addressed. Tel: +49 7071 601 1350; Fax: +49 7071 601 1353; Email: elisa.izaurralde@tuebingen.mpg.de

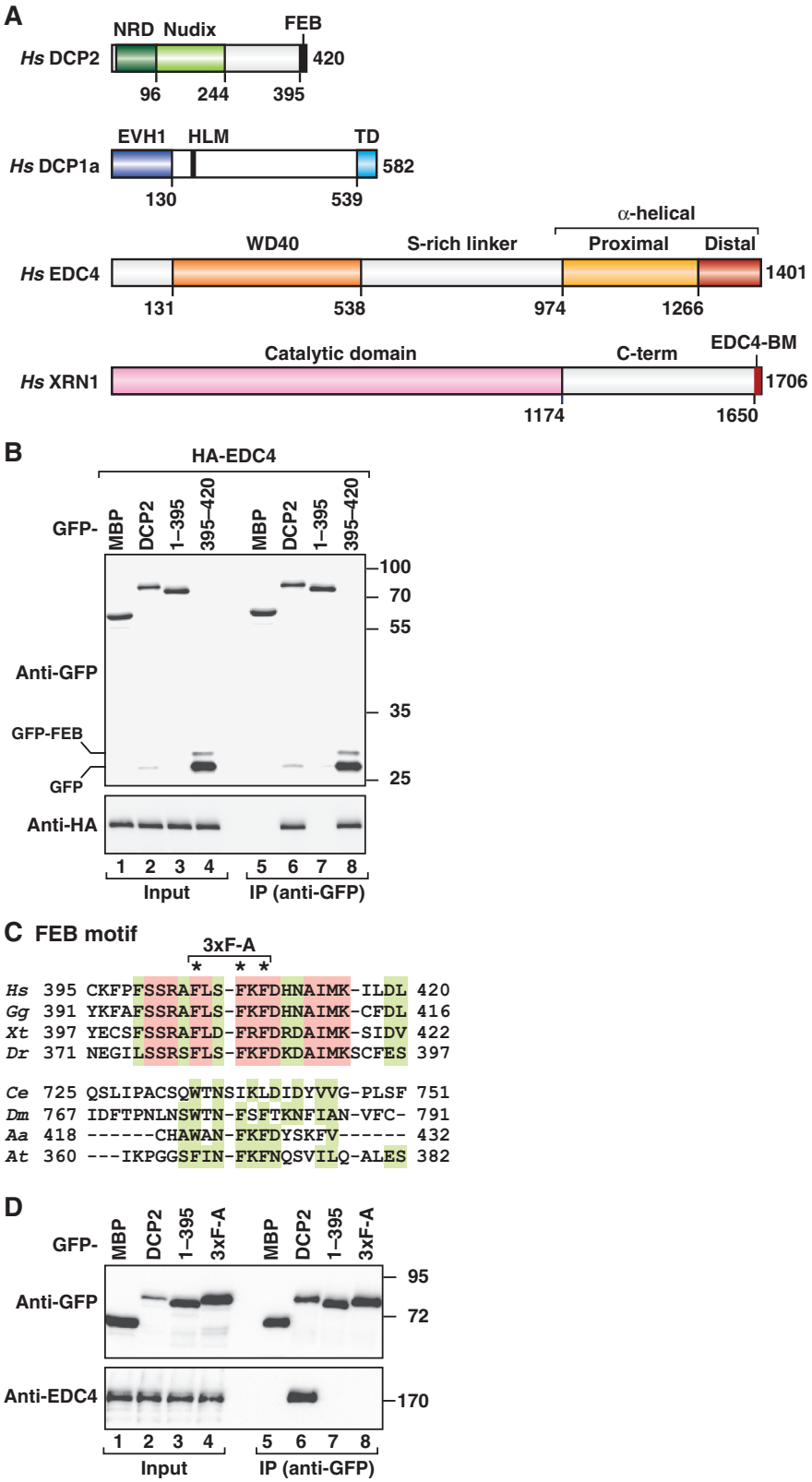

Figure 1. DCP2 interacts with EDC4 via a C-terminal phenylalanine-rich (FEB) motif. (**A**) The domain organization of human DCP2, DCP1a, EDC4 and XRN1. DCP2 consists of an N-terminal regulatory domain (NRD, dark green), a catalytic Nudix domain (light green) and a C-terminal variable region (white). The FEB motif is shown in black. DCP1a consists of an N-terminal EVH1 domain and a C-terminal extension containing a short helical leucine-rich motif (HLM) and a TD. EDC4 consists of a WD40 domain and a α-helical domain connected by a serine-rich linker. XRN1 consists of a catalytic domain and a C-terminal variable region. The EDC4-binding motif (EDC4-BM) in XRN1 is shown in red. The numbers below the protein outlines indicate the residues at the domain boundaries. (**B**) The interaction of GFP-tagged DCP2 (wild type or truncations) with HA-tagged EDC4. The proteins were immunoprecipitated using anti-GFP antibodies. GFP–MBP served as a negative control. Inputs (1%) and

(continued)

factor, EDC4, is required to bridge their interaction (15). Furthermore, EDC4 depletion inhibits decapping in human cells (15).

In addition to the requirement for EDC4, several lines of evidence indicate that the assembly of the decapping complex differs between uni- and multicellular eukaryotes. For example, yeast Dcp1 consists only of an EVH1 domain, whereas in metazoans the DCP1 EVH1 domain is followed by a C-terminal extension (Figure 1A) (4,5,11). This C-terminal extension contains a trimerization domain (TD), which is required for DCP1 binding to DCP2 and EDC4 (16,17), although it is not known how.

Decapping is typically followed by 5′-to-3′ exonucleolytic degradation of the mRNA body by XRN1 (18–20). XRN1 consists of a highly conserved N-terminal catalytic domain and a less conserved C-terminal region (Figure 1A) (21,22). We have previously shown that XRN1-mediated degradation and decapping are coupled through direct interactions between short motifs in the XRN1 C-terminal region and decapping factors (23). In insects, XRN1 interacts with the DCP1 EVH1 domain through a proline-rich DCP1-binding motif (DBM). In vertebrates, XRN1 binds to EDC4 through a C-terminal EDC4-binding motif (EDC4-BM; 23).

The acquisition of EDC4 and of the DCP1 TD, along with the observations that EDC4 oligomerizes (17,24,25), and that XRN1 directly interacts with decapping factors (23), indicates that the composition and stoichiometry of the metazoan decapping complex significantly differs from that of the yeast complex (3). However, until now, studies on the assembly and activation of the decapping complex have been mostly restricted to yeast (1–3). As a result, the molecular basis for the assembly of EDC4, DCP1, DCP2 and XRN1 complexes have not been fully elucidated, and it is not known whether these proteins interact simultaneously or consecutively and whether the mechanism of DCP2 activation is conserved.

To shed light on the assembly of the metazoan decapping complex, we investigate the interactions between DCP1, DCP2, EDC4 and XRN1 in human cells. We show that EDC4 functions as a modular scaffold to provide binding sites for DCP1, DCP2 and XRN1. Thus, EDC4 plays a central role in the assembly of the decapping complex and may facilitate the coordination of decapping with 5′-to-3′ mRNA degradation. We further show that the DCP1 EVH1 domain and the DCP2 NRD form weak but direct interactions that are enhanced by EDC4 and thus, preferentially occur between DCP1 and DCP2 molecules bound on the same EDC4 scaffold. Structural modeling combined with mutagenesis and functional studies identified residues required for complex assembly and mRNA decapping and revealed a role for a conserved loop (which we termed the NR-loop) in the DCP1 EVH1 domain in DCP2 activation.

MATERIALS AND METHODS

DNA constructs

The plasmids for expression of the β-globin-6xMS2bs and the control β-globin-GAP mRNAs were kindly provided by Dr J. Lykke-Andersen and were described previously (26). The plasmids for the expression of DCP1a, DCP2, EDC4, PNRC2, XRN1 and MS2-HA-SMG7 in human cells were described previously (16,23,27). Protein mutants were generated by site-directed mutagenesis using the QuikChange Site-Directed Mutagenesis kit (Stratagene). All constructs were fully sequenced to confirm the presence of the mutations and the absence of additional mutations. Protein mutants used in this study are listed in Supplementary Table S1.

To express the DCP2 395–420 protein fragment with the glutathione *S*-transferase (GST) and maltose-binding protein (MBP) tags in *Escherichia coli*, the corresponding DNA was inserted between the BamHI and NotI restriction sites in the pGEX-6P-1 vector (GE Healthcare) and the XhoI and BamHI sites in the pNEK-NvHM vector (28), respectively. The DNA sequences coding for the XRN1 amino acids 1650–1706 and the EDC4 amino acids 974–1401 were inserted between the EcoRI and XhoI sites of the pGEX-6P-1 vector and the EcoRI and NotI sites of the pETM-41P vector (derived from pETM-41; Novagen), respectively. The DNA sequence coding for DCP2 residues 1–245 was cloned between the XhoI and BamHI sites of the vector pnEA-NpG (28), resulting in an N-terminal GST fusion protein. The DNA coding for the DCP1 EVH1 domain (amino acids 1–130) was cloned behind a His_6-NusA tag between the NdeI–BamHI sites of the vector pnYC-NpHN (28), which already contained a MBP-tagged PNRC2 (amino acids 102–115), resulting in a bicistronic vector.

Structural modeling

To obtain a structural model of the *Hs* DCP1–DCP2 complex, the *Hs* DCP2 sequence was modeled onto the *Sp* Dcp2 structure (PDB code 2QKM) using Phyre (29). The structure of the isolated human EVH1 domain (PDB code 4B6H) was placed relative to DCP2 by superposition with *Sp* Dcp1 from the *Sp* Dcp1–Dcp2 complex structure (PDB code 2QKM). The N-terminal helix of *Hs* DCP1 was superimposed separately onto the *Sp* Dcp1 N-terminal helix. The NR-loop of *Hs* DCP1 formed by amino acids 72–75 was partially unstructured in the isolated human EVH1 domain crystal structure. It was

Figure 1. Continued
bound fractions (IP; 30% and 40% for GFP- and HA-tagged proteins, respectively) were analyzed by western blotting using anti-GFP and anti-HA antibodies. (**C**) A sequence alignment of the FEB motif. The residues conserved in all aligned vertebrate sequences are shown with a salmon background, and residues with >70% similarity are highlighted in green. The asterisks indicate the residues mutated in the 3xF-A mutant. The species abbreviations are as follows: *Hs* (*Homo sapiens*), *Gg* (*Gallus gallus*), *Xt* (*Xenopus tropicalis*), *Dr* (*Danio rerio*), *Ce* (*Caenorhabditis elegans*), *Dm* (*Drosophila melanogaster*), *Aa* (*Aedes aegypti*), *At* (*Arabidopsis thaliana*). (**D**) The interaction of GFP–DCP2 (wild type or mutants) with endogenous EDC4. The size markers (kDa) are shown on the right of each panel.

therefore modeled based on *Sp* Dcp1 using Phyre. The ATP molecule was taken from the *Sp* Dcp1–Dcp2 complex structure and placed by superimposition.

Coimmunoprecipitation assays and western blotting

For coimmunoprecipitation assays, HEK293T cells were grown in 10-cm dishes and transfected using either the calcium phosphate method or Lipofectamine 2000 (Invitrogen). The cells were transfected with 15 to 24 μg of total plasmid DNA. Two days after transfection, the cells were washed with phosphate-buffered saline and lysed on ice for 15 min in 1 ml of NET buffer (50 mM Tris (pH 7.5), 150 mM NaCl, 1 mM EDTA, 0.1% Triton-X-100 and 10% glycerol and supplemented with protease inhibitors) per dish. Immunoprecipitations were performed as described previously (23). The cell lysates were treated with RNase A prior to immunoprecipitation in all experiments. Antibodies used in this study are listed in Supplementary Table S2. All western blots were developed with the ECL western blotting detection system (GE Healthcare), as recommended by the manufacturer.

Pulldown assays

The recombinant proteins used in pulldown assays were separately expressed in *E. coli* BL21 (DE3) STAR cells using ZY autoinduction media at 20°C overnight (30). The pulldown assays were performed as described previously (23) in RB100 buffer (25 mM HEPES (pH 7.5), 100 mM KOAc, 10 mM $MgCl_2$, 1 mM 1,4 Dithiothreitol (DTT), 0.05% Triton-X-100 and 10% glycerol) containing RNase A (10 μg/ml). The purified proteins were incubated with 10 μl (50% slurry) of Protino Glutathione Agarose 4B beads (Macherey Nagel). The bound proteins were washed with RB100 buffer, eluted with 2× protein sample buffer and analyzed by 12% sodium dodecyl sulphate-polyacrylamide gel electrophoresis (SDS-PAGE) followed by Coomassie brilliant blue staining.

For the pulldown of purified DCP1 by DCP2 shown in Figure 5C, GST or GST–DCP2 (amino acids 1–245; wild type or the D15A,R19A mutant) were expressed in BL21 (DE3) STAR cells in LB medium at 20°C overnight. After cell lysis by sonication in buffer containing 50 mM HEPES (pH 7.5), 200 mM NaCl, 5% glycerol and 2 mM DTT supplemented with lysozyme, DNase I and protease inhibitors, proteins were affinity purified using glutathione agarose beads. Finally, contaminating proteins were removed by size exclusion chromatography using a superdex 200 column (GE Healthcare). His_6–NusA–DCP1 (amino acids 1–130) was coexpressed with MBP–PNRC2 (amino acids 102–115) to stabilize DCP1 (31). Cells were lysed by sonication in a buffer containing 50 mM HEPES (pH 7.5), 200 mM NaCl, 20 mM imidazole, 2 mM β-mercaptoethanol, lysozyme, DNase I and protease inhibitors. After initial Ni-affinity purification using an IMAC-column (GE Healtcare) the two proteins were finally copurified using a superdex 200 column.

GST-pulldowns using these purified proteins were carried out in pulldown buffer (PD) containing 50 mM HEPES (pH 7.5), 200 mM NaCl, 2 mM DTT. Mixtures of 25 μl glutathione agarose beads, 10 μM NusA–DCP1/MBP–PNRC2 complex and 10 μM GST or GST–DCP2 (wild type or mutant) in 75 μl PD buffer were incubated at 4°C for 30 min. The beads were washed three times with 750 μl of pulldown buffer. Bound proteins were subsequently eluted with 30 μl PD buffer containing 25 mM glutathione and analyzed by SDS-PAGE.

Tethering assays

Tethering assays using the MS2-reporter system were performed as described previously (27). Briefly, HEK293T cells were cultured in 6-well plates and transiently transfected with a mixture of four plasmids: 0.5 μg of the control plasmid (β-globin-GAP), 0.5 μg of the plasmid encoding the β-globin-6xMS2bs, 0.5 μg of plasmids expressing the MS2–HA fusion protein (SMG7 or the TNRC6A silencing domain, amino acids 925–1709) and 2 μg of plasmids encoding GFP–DCP2 (wild type or mutant) or GFP–DCP1 (wild type or mutant). RNase H (New England Bioloabs) digestion was carried out as described previously (27).

Decapping assays

The decapping assays were performed as described previously (16) in decapping buffer containing 50 mM Tris–HCl (pH 7.5), 50 mM ammonium sulfate and 5 mM $MgCl_2$. Reactions were stopped by adding up to 50 mM EDTA and analyzed on PEI cellulose thin-layer chromatography plates (Merck) in 0.75 M LiCl (1 μl/sample). The *in vitro* synthesized RNA (127 nucleotides) probe was labeled with [γ-^{32}P]GTP using the ScriptCap m^7G Capping System and the ScriptCap 2'-*O*-Methyltransferase kit (EPICENTRE Biotechnologies).

RESULTS

A conserved phenylalanine-rich motif in DCP2 mediates binding to EDC4

The decapping enzyme DCP2 interacts with DCP1 and EDC4 in human cells (15). Using a fluorescence-based two-hybrid assay, it has been shown that DCP2 and EDC4 interact via their C-terminal regions (17). Using coimmunoprecipitation as an alternative method, we identified a short DCP2 C-terminal motif comprising residues 395–420 to be both necessary and sufficient for binding to EDC4 in an RNA independent manner in human cells (Figure 1B, lane 8). The remaining DCP2 fragment (residues 1–395) did not interact with EDC4 at detectable levels (Figure 1B, lane 7).

Analysis of the DCP2 sequence revealed that residues 395–420 are highly conserved in vertebrates and feature three invariant phenylalanine residues (F404, F407 and F409; Figure 1C). Remarkably, alanine substitution of these three phenylalanine residues (3×F-A) in the full length DCP2 abolished the interaction with endogenous EDC4 as efficiently as the deletion of the entire motif (Figure 1D, lane 8 vs. 7). We conclude that DCP2 interacts with EDC4 via a conserved C-terminal phenylalanine-containing motif comprising residues 395–420, which we

termed the phenylalanine-rich EDC4-binding (FEB) motif (3).

The FEB motif interacts directly with the EDC4 C-terminal α-helical domain

Next, we used a similar deletion analysis for EDC4 to define the minimal region required for DCP2 binding. EDC4 consists of a predicted N-terminal WD40 domain and a C-terminal α-helical domain connected by a serine-rich linker (Figure 1A) (15,24,25,32). In agreement with previous studies (17,24), DCP2 interacted with the EDC4 C-terminal α-helical domain (residues 974–1401; Figure 2A, lane 16).

To investigate whether the interaction of the DCP2 FEB motif with the EDC4 α-helical domain is direct, we performed pulldown assays with purified recombinant proteins expressed in *E. coli*. The DCP2 FEB motif (residues 395–420) was expressed with a GST tag, and the α-helical domain of EDC4 (974–1401) was fused to the MBP. We observed that GST–FEB, but not GST alone, pulled down MBP–EDC4 on glutathione–agarose beads (Figure 2B, lane 3 vs. 2), indicating that the interaction is direct.

EDC4 interacts directly and simultaneously with DCP2 and XRN1

In our previous work, we demonstrated that the EDC4 C-terminal domain interacts directly with a short motif in the vertebrate XRN1 C-terminal region (termed EDC4-BM, Figure 1A) (23). We therefore asked whether

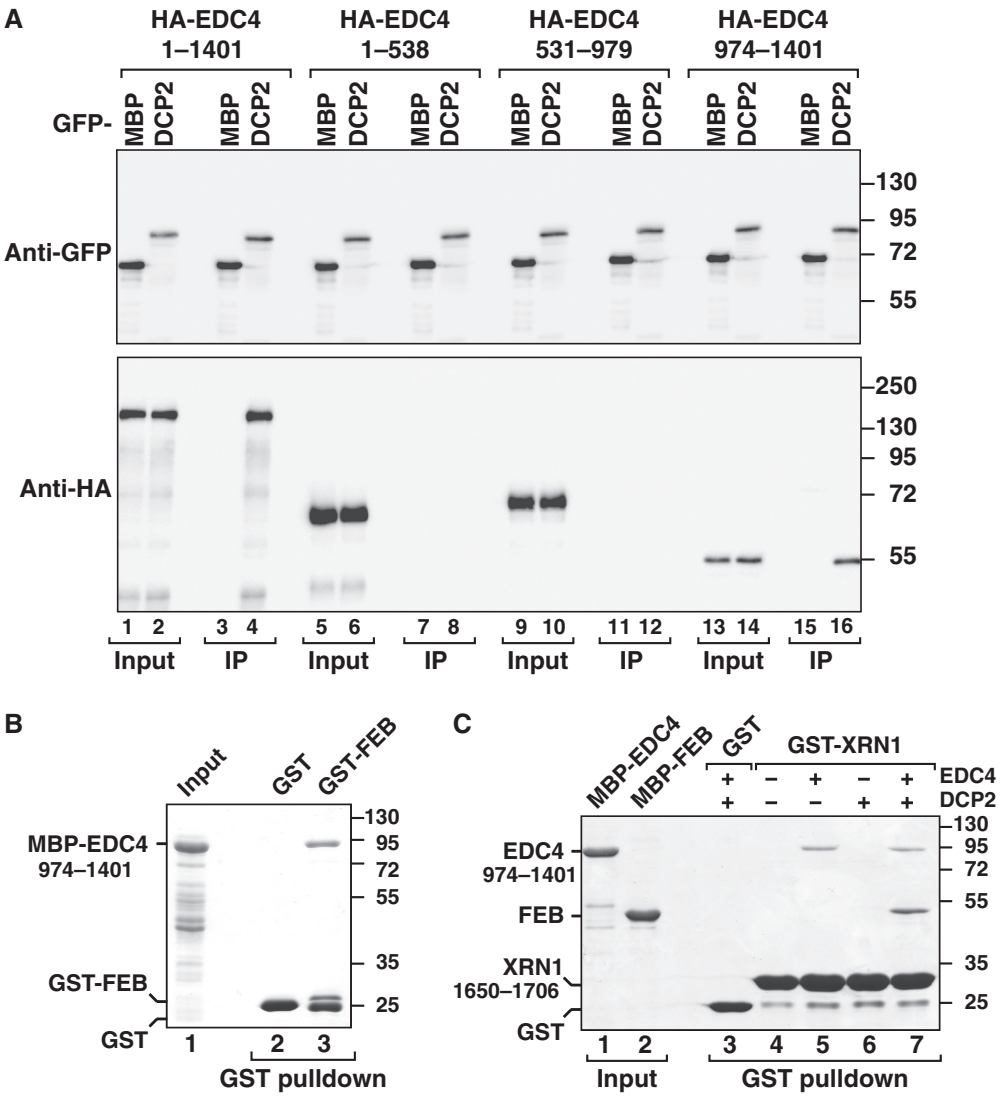

Figure 2. EDC4 interacts simultaneously with the DCP2 FEB motif and the XRN1 EDC4–BM. (**A**) The interaction of GFP–DCP2 with HA–EDC4 (full length or the indicated fragments). The proteins were immunoprecipitated using anti-GFP antibodies and analyzed as described in (**Figure 1B**). (**B**) A GST pulldown assay showing the interaction of the GST–FEB motif (DCP2 residues 395–420) with the recombinant MBP–EDC4 (residues 974–1401). GST served as a negative control. (**C**) A GST pulldown showing the interaction of GST–XRN1 (residues 1650–1706) with recombinant MBP–EDC4 (residues 974–1401) and MBP–FEB motif. GST served as a negative control. The size markers (kDa) are shown on the right of each panel.

EDC4 binds DCP2 and XRN1 simultaneously. We observed that a GST-tagged version of the XRN1 motif (residues 1650–1706) pulled down the MBP-tagged EDC4 α-helical domain (EDC4 residues 974–1401; Figure 2C, lane 5), as expected (23). Furthermore, the XRN1 motif also pulled down the purified DCP2 FEB motif in the presence of EDC4 but not in its absence (Figure 2C, lane 7 vs. 6). These results indicate that EDC4 bridges the DCP2-XRN1 interaction. We conclude that the DCP2 FEB motif and the XRN1 EDC4-BM bind simultaneously to the EDC4 α-helical domain and thus do not compete for the same binding surface, in agreement with the observation that these motifs do not exhibit sequence similarity (Figure 1C; Supplementary Figure S1A).

Structural information is only available for the distal portion of the EDC4 α-helical domain (Figure 1A) (25). To determine whether this region binds to XRN1 and DCP2 we performed coimmunoprecipitation assays with two non-overlapping EDC4 C-terminal fragments. Notably, both XRN1 and DCP2 interacted with the proximal portion of the domain (EDC4 residues 974–1265; Figure 3A and B, lanes 8), for which no structure

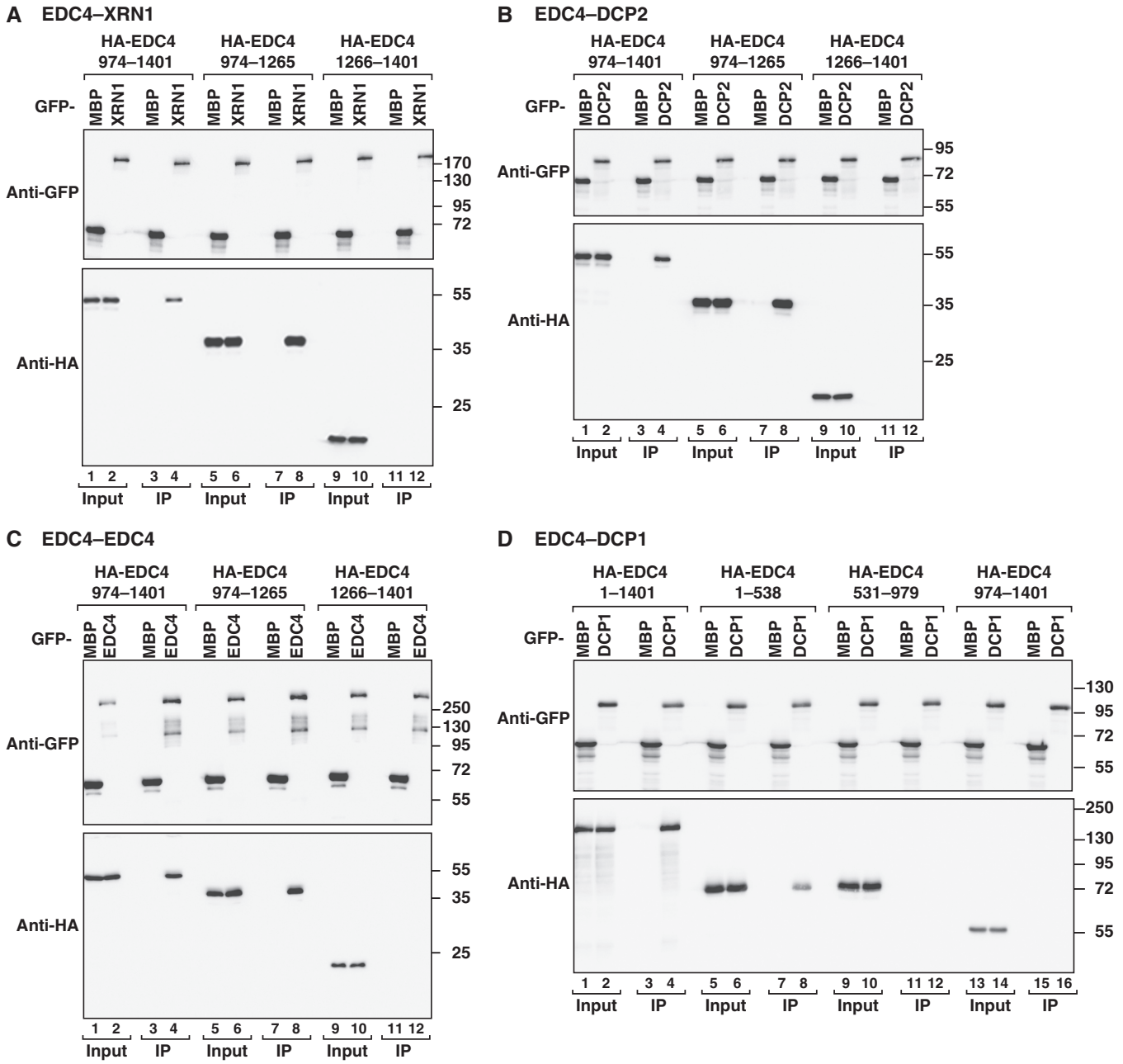

Figure 3. EDC4 multimerization and its interaction with XRN1, DCP2 and DCP1. (**A–D**) The interactions of HA-EDC4 (full-length or the indicated fragments) with GFP–XRN1 (**A**), GFP–DCP2 (**B**), GFP–EDC4 (**C**) and GFP–DCP1a (**D**). The proteins were immunoprecipitated using anti-GFP antibodies. GFP–MBP served as a negative control. The inputs (1.5% and 0.5% for the GFP- and HA-tagged proteins, respectively) and bound fractions (IP; 30% and 20% for the GFP- and HA-tagged proteins, respectively) were analyzed by western blotting. The size markers (kDa) are shown on the right of each panel.

is available. Additionally, this region mediated EDC4 homo-oligomerization (Figure 3C, lane 8), as reported previously (17,24).

In summary, the proximal portion of the EDC4 α-helical domain is an oligomerization domain that binds directly and simultaneously to DCP2 and XRN1 and thus may link decapping to 5′-to-3′ mRNA degradation in human cells.

DCP1 interacts with the EDC4 WD40 domain independently of DCP2

In addition to its interaction with DCP2 and XRN1, EDC4 also interacts with DCP1, although it is not clear how (15–17,24,25). Studies in human cells indicated that the EDC4 C-terminal α-helical domain binds to DCP1 and therefore this interaction could be mediated by DCP2 (17). However, in *Arabidopsis thaliana*, the EDC4 C-terminal region was not sufficient for DCP1 binding *in vitro* (24).

To resolve this apparent discrepancy, we tested which domains of EDC4 are required for DCP1 binding in human cells. We observed that the N-terminal WD40 domain interacted with DCP1, although not as efficiently as full length EDC4 (Figure 3D, lane 8 vs. 4). In contrast, the EDC4 C-terminal region, which binds directly DCP2 (Figure 2B), did not detectably interact with DCP1 (Figure 3D, lane 16). Collectively, our results indicate that EDC4 provides independent binding sites for DCP1, DCP2 and XRN1 and thus functions as a scaffold for complex assembly (see model in Figure 9).

The interaction of DCP2 with DCP1 requires the NRD and the FEB motif

Having defined how EDC4 interacts with DCP1 and DCP2, we next investigated the DCP1–DCP2 interaction. We observed that GFP-DCP2 coimmunoprecipitated with HA-tagged DCP1 in an RNA-independent manner (Figure 4A, lane 10) (4). This interaction was reduced when the DCP2 NRD was deleted (DCP2 residues 97–420), indicating that this domain contributes to DCP1 binding (Figure 4A, lane 11). Remarkably, the deletion of the FEB motif or the 3×F-A substitutions also strongly impaired DCP2 binding to DCP1 (Figure 4A, lanes 12 and 15, respectively). The residual binding to DCP1 observed for these DCP2 mutants may reflect a weak interaction mediated by the DCP2 NRD. Consistent with this hypothesis, a DCP2 fragment lacking both the NRD and the FEB motif did not interact with DCP1 at detectable levels (residues 97–395; Figure 4A, lane 13).

Our results indicate that in contrast to the interaction between the yeast proteins, the interaction between human DCP1 and DCP2 requires both the DCP2 NRD and the FEB motif. Because the FEB motif directly binds EDC4 (Figure 2B), its contribution to DCP1 binding is most likely indirect and mediated by EDC4.

The DCP2 NRD interacts with the DCP1 EVH1 domain

Because of the poor sequence conservation of DCP1 interface residues it has been proposed that DCP1 does not bind DCP2 directly in metazoans but that this interaction is bridged by EDC4 (1,3). However, our observation that the DCP2 NRD contributes to DCP1 binding suggests that this domain may interact with the DCP1 EVH1 domain using a binding mechanism similar to that described for the yeast proteins (10). Nevertheless, this binding may be weak and may require stabilization by EDC4 (3,15), as evidenced by the weak interaction observed for DCP2 mutants impaired in EDC4 binding (Figure 4A, lanes 12 and 15). To test this hypothesis, we generated a model based on the high-resolution structure of the *Sp* Dcp1–Dcp2 complex (10). The NRD and the Nudix domain of human and *Sp* DCP2 exhibit 41% and 45% identity, respectively, and the DCP1 EVH1 domains are 30% identical and share good structural homology (RMSD = 1.4 Å over 105 Cα atoms) (10,31). Thus, a reliable model for the human complex can be obtained.

Sp Dcp2 uses residues in helices α1 and α2 and in loop L3 of the NRD to interact with Dcp1 residues in helix α1 and in a conserved loop of the EVH1 domain that we termed the NR-loop (Figure 4B and C, Supplementary Figure S1B and C) (10,31). The main interaction interface is between the α1 helices of both *Sp* Dcp1 and Dcp2 (Figure 4D and E). The Dcp2 interface residues are highly conserved (Figure 4B and E). Specifically, human DCP2 residues D15 and R19 in helix α1 (corresponding to *Sp* Dcp2 D14 and R18) are predicted to form hydrogen bonds with the DCP1 residues H19 in helix α1 and N77 in the NR-loop (*Sp* Dcp1 H19 and N76), respectively (Figure 4B, C and E).

In contrast to DCP2, the DCP1 residues in helix α1 involved in DCP2 binding are not well conserved (Figure 4C; Supplementary Figure S1C). Nevertheless, the residues at structurally equivalent positions are likely to contact DCP2 through a network of hydrogen bonds and hydrophobic interactions. For example, in addition to residue H19, residues S12 and Q18 are predicted to form hydrogen bonds with residues H23 and S11, respectively, in the DCP2 α1 helix (Figure 4E). However, several intermolecular hydrogen bonds and hydrophobic contacts present in the *Sp* structure are lost in the human proteins, which might explain the weaker binding of the human orthologs. In particular, the *Sp* Dcp2 residue K77 (in loop L3), which makes two hydrogen bonds to Dcp1, is replaced by a proline residue in human DCP2 (P78, Figure 4B and E). Instead of the two hydrogen bonds between the *Sp* Dcp2 N22 and the Dcp1 N12 residues, only one bond could be formed in the human proteins between the equivalent H23 and S12 residues (Figure 4E). *Sp* Dcp1 Q14, which makes a hydrogen bond to Dcp2 D13, is substituted with alanine in human DCP1 (Figure 4C). Furthermore, the *Sp* Dcp1 L7 and V15 residues involved in hydrophobic interactions are replaced by alanine residues in the human DCP1 (Figure 4C and E).

To validate the structural model, we generated mutations in DCP2 to disrupt the predicted interface. We observed that alanine substitution of the DCP2 residues D15 and R19 reduced the binding to DCP1 to a similar extent as the deletion of the entire NRD (Figure 4A, lane 14 vs. 11; D,R). These results indicate that the DCP2 NRD contacts DCP1 using equivalent residues in the

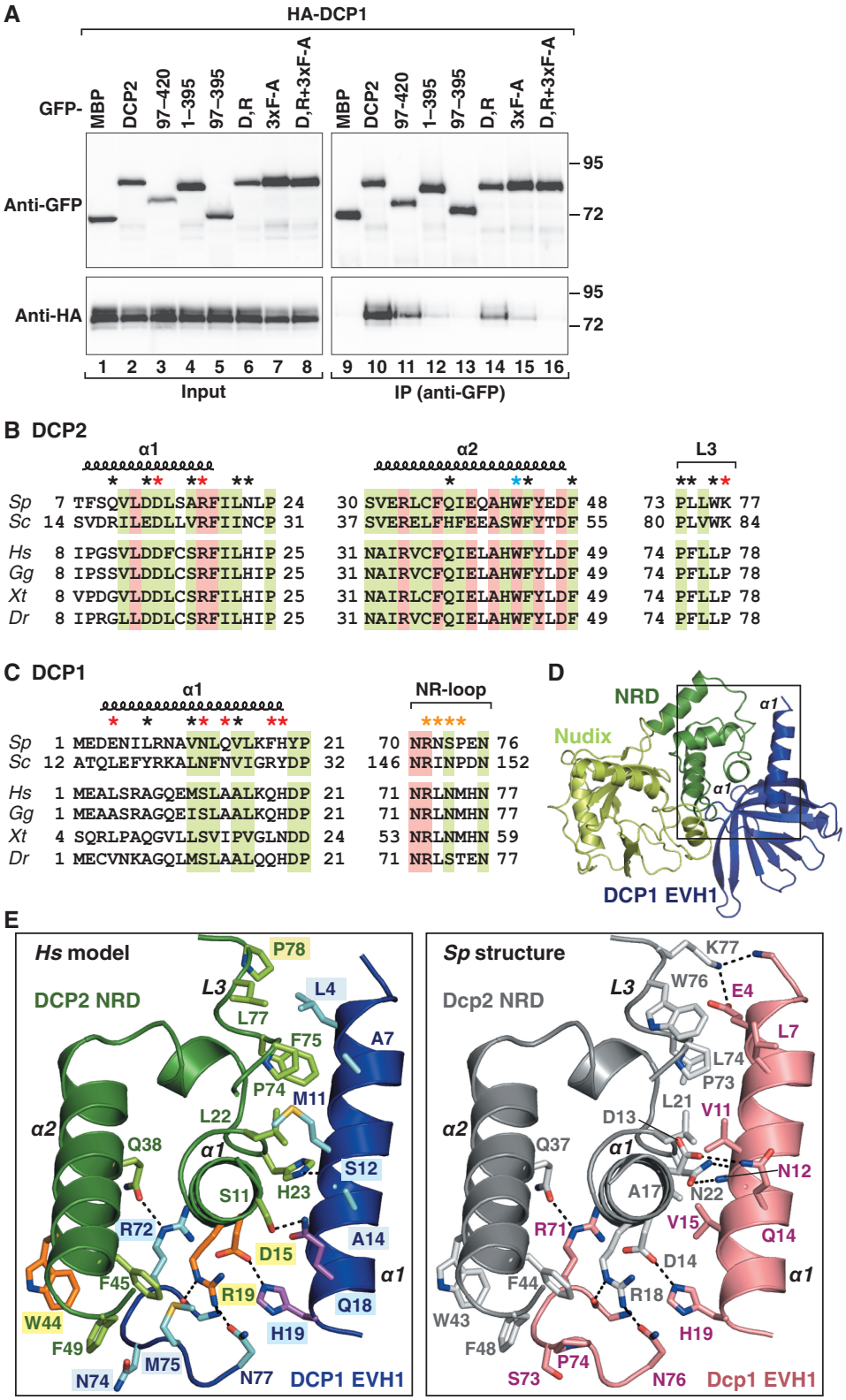

Figure 4. The interaction of DCP2 with DCP1 requires the NRD and the FEB motif. (**A**) The interaction of GFP–DCP2 (wild type or mutant) with HA–DCP1a. The samples were analyzed as described in Figure 1B. (**B** and **C**) Sequence alignments of the regions of DCP2 (**B**) and DCP1 (**C**) involved in complex formation. The colors and species abbreviations are as indicated in Figure 1C. The secondary structure elements of the *Sp* Dcp2 and *Hs* DCP1 structures are indicated above the alignments. The residues at the DCP1–DCP2 interface are marked by black and red asterisks. The red asterisks mark the interface residues mutated in this study. The 'gatekeeper' tryptophan (W44) is labeled with a cyan asterisk. The NR-loop residues mutated in this study are indicated with orange asterisks. The alignments including additional species are shown in Supplementary Figure S1. (**D**) A model of the human DCP1–DCP2 complex based on the *Sp* Dcp1–Dcp2 co-crystal structure (10). The DCP1 EVH1 domain is shown in blue, the DCP2 NRD is shown in dark green, and the Nudix domain is shown in light green. The rectangle indicates the view shown in panel (E).

(continued)

human and yeast proteins. DCP2 binding to DCP1 was abolished when the D15A and R19A mutations in the NRD were combined with mutations in the FEB motif that disrupt EDC4 binding (Figure 4A, lane 16; mutant D,R+3xF-A). These combined mutations had a similar effect as the deletion of the NRD and the FEB motif (Figure 4A, lanes 16 and 13). Thus, the DCP2 NRD contacts the DCP1 EVH1 domain using equivalent amino acids in human as in yeast, and this binding is enhanced by EDC4, which provides a major contribution to the interaction.

DCP1 and DCP2 directly interact

Next, we generated mutations in the DCP1 EVH1 domain to disrupt DCP2 binding. We observed that the DCP1–DCP2 interaction was strongly impaired when at least two proposed interface residues (i.e. Q18 and H19 or S12 and H19) were substituted by alanine (Figure 5A; lanes 12 and 13; Q,H and S,H), whereas the H19A substitution alone was ineffective (Figure 5A, lane 11). The combined S12A, Q18A and H19A substitutions abolished DCP2 binding (Figure 5A, lane 14) and slightly reduced EDC4 binding (Figure 5B, lane 14). As a negative control, we used mutations that prevent DCP1 trimerization (Mut1), which abolished DCP2 binding and strongly reduced EDC4 binding as previously reported (Figure 5A and B, lane 10) (16). It is not known how the trimerization mutant affects DCP2 binding (3,16).

To further validate the structural model, we substituted residues in human DCP2 and DCP1 to mimic the yeast interface. In particular we introduced a P78K substitution in DCP2 and a L4E,A14Q substitution in DCP1. These substitutions increased the affinity of the DCP1–DCP2 interaction (Supplementary Figure S1E), but only when they were combined by mutations that disrupt EDC4 binding. These results indicate that the interaction mediate by EDC4 provides a major contribution to the formation of the DCP1–DCP2 complex.

To investigate whether human DCP1 and DCP2 indeed bind each other directly, we performed pulldown assays *in vitro* with purified recombinant proteins expressed in *E. coli*. The DCP2 fragment containing the NRD and the Nudix domain (residues 1–245) was expressed with a GST tag. The DCP1 EVH1 domain (residues 1–130) was expressed with a hexa-histidine tag fused to NusA (as a solubility tag) and was further stabilized by coexpressing the PNRC2 binding peptide (residues 102–115) fused to MBP. The PNRC2 peptide binds to the hydrophobic cleft of the DCP1 EVH1 domain and facilitates its purification (31). DCP2 and the DCP1–PNRC2 complex were purified separately and mixed in a 1:1 ratio (Figure 5C, lanes 1–3). The protein complexes were pulled down with glutathione–agarose beads.

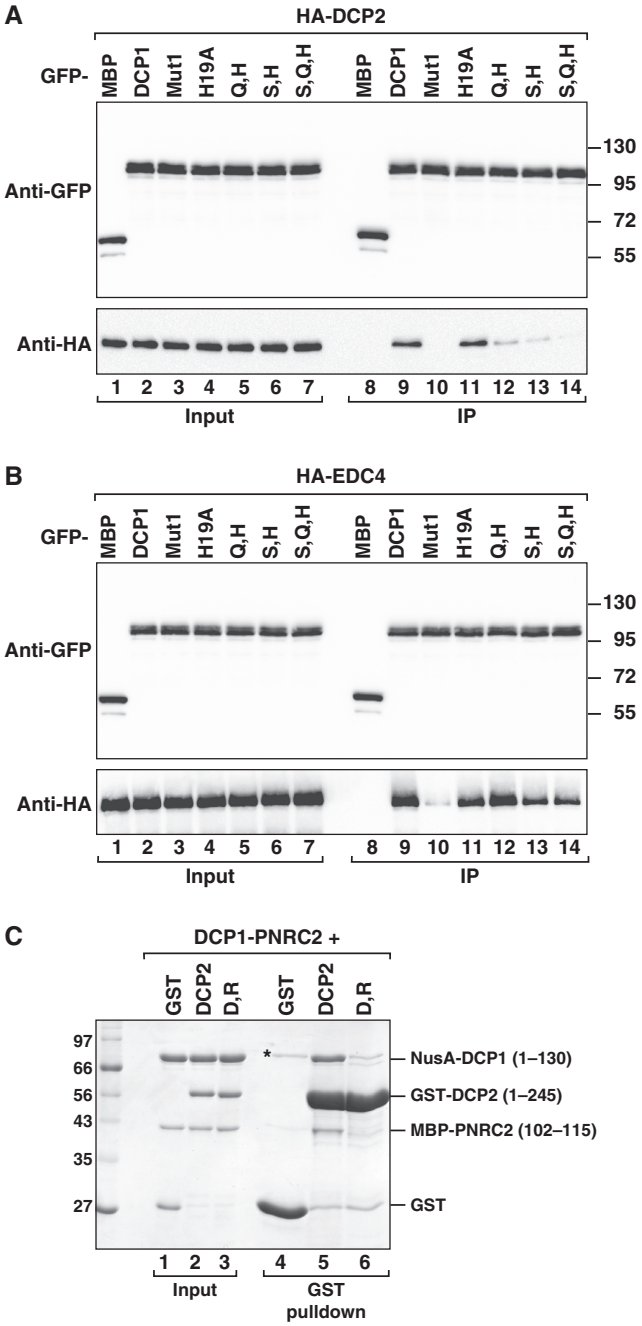

Figure 5. DCP1 and DCP2 directly interact. (**A** and **B**) The Interactions of GFP–DCP1a (wild type or mutants) with HA–DCP2 (**A**) and HA–EDC4 (**B**). Inputs (1.5% and 1% for the GFP- and HA-tagged proteins, respectively) and bound fractions (IP; 30% and 20% for the GFP- and HA-tagged proteins, respectively) were analyzed by western blotting. (**C**) A GST pulldown assay showing the interaction of GST–DCP2 (residues 1–245) with the recombinant His_6–NusA–tagged DCP1a EVH1 domain (residues 1–130) bound to MBP-tagged PNRC2 (residues 102–115). GST served as a negative control. The asterisk indicates a protein copurifying with GST.

Figure 4. Continued
(**E**) A model of the human DCP1–DCP2 interface (left panel) based on the *Sp* Dcp1–Dcp2 co-crystal structure (right panel) (10). The putative interface residues for the human proteins are shown as sticks in cyan (DCP1) or green (DCP2). The residues mutated in this study are labeled with a cyan (DCP1) and yellow (DCP2) background. DCP1 residues Q18 and H19 are highlighted in purple. DCP2 residues D15, R19 and W44 are highlighted in orange (DCP2). The 'gatekeeper' tryptophan (W44) is shown in the orientation observed in the closed conformation. Secondary structural elements are indicated in italics.

We observed that DCP2 pulled down the DCP1–PNRC2 complex (Figure 5C, lane 5). The interaction was weak, and only sub-stoichiometric amounts of the DCP1 complex were pulled down. Nevertheless, the interaction was specific, as it was strongly reduced by the D15A and R19A substitutions in DCP2 (Figure 5C, lane 6). Collectively, our results indicate that the interaction between the DCP1 EVH1 domain and the DCP2 NRD is direct, but the binding affinity is low, presumably due to substitutions of the interface residues in human DCP1. This loss of affinity is, at least in part, compensated by an additional indirect interaction mediated by EDC4.

DCP2 activation by DCP1 requires interface residues and the FEB motif

To further investigate the relevance of the interactions involving DCP1 and EDC4 for DCP2 function, we tested the decapping activity of the aforementioned DCP2 mutants *in vitro*. Immunopurified GFP–DCP2 exhibited decapping activity (Figure 6A, lanes 2–4 and Figure 6B), as reported previously (4,16). This activity was specific because a DCP2 protein variant that carries a glutamine substitution in one of the four catalytic glutamates (E148Q) was strongly impaired (Figure 6A, lanes 5–7 and Figure 6B), as expected (4,9,33). A western blot carried out with the corresponding samples showed that wild-type DCP2 and the E148Q mutant interacted with DCP1 and EDC4 to comparable levels and that equivalent amounts of immunoprecipitated DCP2 were present in the decapping reaction (Figure 6C, lanes 2 and 3).

The disruption of the DCP2 interaction with EDC4 had a modest effect on the decapping activity *in vitro* (Figure 6A, lanes 11–13 and Figure 6B, mutant 3xF-A). Accordingly, a reduced amount of DCP1 was detectable in the reaction (Figure 6C, lane 5). In contrast, the decapping activity was strongly impaired when DCP1 binding was prevented by the combined D15A and R19A mutations (Figure 6A, lanes 8–10; Figure 6B; mutant D,R), although the amount of endogenous EDC4 present in the reaction was not affected (Figure 6C, lane 4). DCP2 decapping activity was further inhibited when the D15A and R19A mutations were combined with the 3xF-A mutations (D,R+3xF-A; Figure 6A, lanes 14–16 and Figure 6B). These results indicate that DCP2 activation by DCP1 requires the interaction between the DCP2 NRD and the DCP1 EVH1 domain.

Conservation of the DCP2 catalytic mechanism

Given that the EVH1 domain of human DCP1 interacts with the DCP2 NRD, that this interaction contributes to DCP2 decapping activity and that DCP2 is highly conserved, we expected that the mechanisms underlying catalysis and DCP2 activation by DCP1 are conserved. To test this hypothesis, we designed mutations that are predicted to interfere with catalysis and activation without affecting the DCP1–DCP2 interaction.

In particular, a structural feature in *Sp* Dcp2 that plays a key role in activation is the hinge region (*Hs* DCP2 residues K94 to V97) between the NRD and the Nudix domain that allows for conformational changes between the two domains (Figure 6D and E; Supplementary Figure S1D) (10,13,14). Accordingly, the substitution of any of the hinge residues with proline in the *Sp* and *Sc* Dcp2 rigidifies the hinge region, prevents the open-to-closed transitions and inhibits decapping both *in vitro* and *in vivo* (10).

Therefore, we substituted residues G96 and V97 in human DCP2 with proline residues and tested for decapping activity *in vitro* and for binding to DCP1 and EDC4 in coimmunoprecipitation assays. We observed that the DCP2 G96P,V97P mutant inhibited decapping activity to a similar extent as the E148Q mutation (Supplementary Figure S2A and B). This mutant retained EDC4 binding (Figure 6F, lane 11; G,V) but surprisingly, was consistently impaired in DCP1 binding (Figure 6G, lane 11 and data not shown). Thus, the flexibility of the hinge region is required for binding and activation by DCP1.

Another feature required for catalysis and DCP2 activation by DCP1 in yeast is the invariant W44 residue (*Sp* Dcp2 W43) a component of the active site located in the DCP2 helix α2 (Figures 4B and E and 6H). This residue flips the orientation between the open and closed DCP2 conformations (Figure 6H, in yellow and orange, respectively) (10). NMR studies indicated that the substitution of *Sp* Dcp2 W43 with alanine abolishes the open-to-closed transitions and hence prevents DCP2 activation by DCP1, suggesting that it functions as a 'gatekeeper' residue (14).

We observed that alanine substitution of W44 in human DCP2 abolished decapping activity as efficiently as the E148Q mutation (Supplementary Figure S2A and B). A western blot analysis demonstrated that comparable amounts of DCP2 were present in the decapping reaction (Supplementary Figure S2B). Because the W44A mutation did not interfere with DCP1 or EDC4 binding (Figures 6F and 6G, lanes 10) but did inhibit decapping, we conclude that W44 is required for DCP2 catalytic activity as observed for the yeast protein (14).

Finally, we also substituted the invariant K130 residue in the Nudix domain with alanine, as this residue was shown to play a key role in catalysis, most likely by contacting one of the phosphates of the cap and positioning it for catalysis (Figure 6H) (10,12,33). This substitution abolished DCP2 decapping activity and also slightly reduced DCP1 but not EDC4 binding (Supplementary Figure S2A and B; Figure 6F and G). Collectively, these results indicate conservation of the catalytic and activation mechanisms.

A conserved loop in the DCP1 EVH1 domain is required for DCP2 activation

Next, we sought to design mutations in DCP1 that do not affect DCP2 binding but may affect its DCP2-activation function. Residues in the NR-loop of the DCP1 EVH1 domain have been proposed to promote conformational changes in DCP2 that favor the active closed conformation (10). Consistent with an important role for this loop, residues N71 and R72 are invariant (Figure 4C;

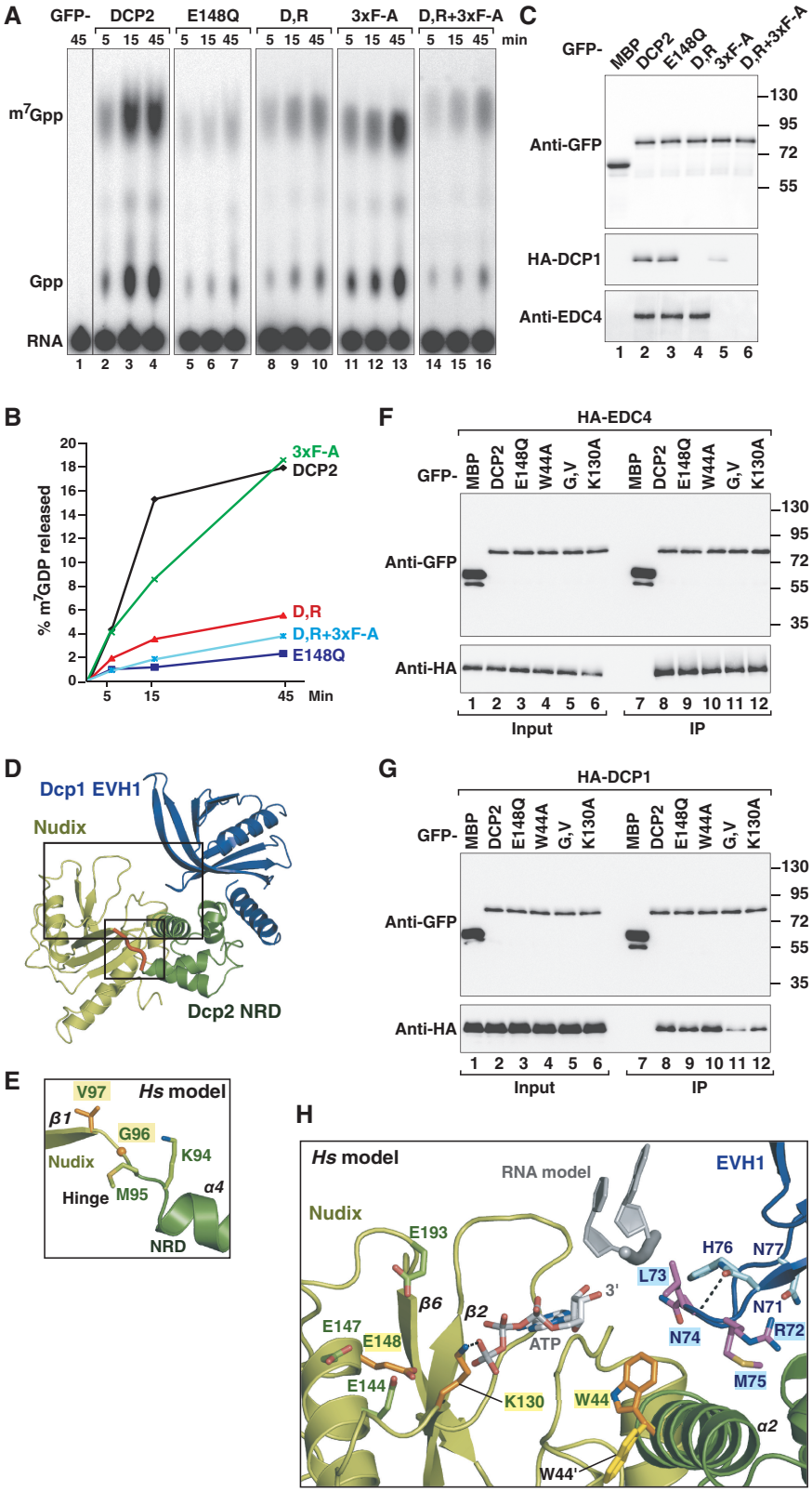

Figure 6. Decapping by DCP2 requires an interaction with DCP1 and EDC4. (**A**,**B**) GFP–DCP2 proteins (wild type or mutants) were expressed in human HEK293T cells. The proteins were immunopurified using anti-GFP antibodies and tested for decapping activity *in vitro*. GFP–MBP served as a negative control. The decapping reaction was terminated at the indicated time points by addition of EDTA and analyzed on PEI cellulose thin-layer chromatography plates. The m^7GDP signal was quantified and normalized to that of the total signal (capped RNA+ m^7GDP signal) for each protein. In (**B**) these normalized values were plotted against time. Gpp is produced in the reactions due to incomplete methylation of the capped mRNA. (**C**) The samples corresponding to panel (A) were analyzed by Western blotting using the indicated antibodies. (**D**) An overview of the model of the human DCP1–DCP2 complex. The small and large rectangles indicate the views shown in (**E**) and (**H**), respectively. The colors are

(continued)

Supplementary Figure S1C), and thus we termed this loop the NR-loop (asparagine–arginine loop).

By analogy to the *Sp* Dcp1–Dcp2 structure, the peptide backbone of N71 likely establishes hydrogen bonds with DCP2 residue R19 in helix α1 (Supplementary Figure S2C) and thus could contribute to the DCP1–DCP2 interaction. Furthermore, the conformation and flexibility of the NR-loop are constrained by a number of intra- and intermolecular hydrogen bonds (Supplementary Figure S2C). The side chain of residue N71 is predicted to bind to the backbone of the NR-loop residue L73. Residue R72 is predicted to form two hydrogen bonds to DCP2, one with residue Q38 in helix α2 and one with the backbone oxygen of the F20 residue in helix α1. Finally, residue N77 at the end of the loop is predicted to interact with the DCP2 R19 (Supplementary Figure S2C). In this fixed conformation, the side chains of loop residues L73, N74 and H76 project toward the RNA substrate-binding channel (Figure 6H).

To investigate the role of the NR-loop, we substituted residues R72 and N74 with glycine residues individually or in combination. We also replaced four loop residues (R72 to M75) with a GSSG linker, which forms a flexible loop and is unlikely to adopt a fixed conformation. None of these substitutions affected the interactions of DCP1 with DCP2 or EDC4 (Figure 7A and B), indicating that they do not disrupt the DCP1 fold and that the NR-loop does not provide a major contribution to these interactions. Furthermore, the substitutions in the NR-loop did not prevent the interaction with PNRC2 (Supplementary Figure S2D), indicating that the EVH1 domain fold was not affected.

To test the effects of the NR-loop mutations on the activity of the decapping complex, we performed decapping assays *in vitro*. DCP1 coimmunopurifies with decapping activity (Figures 7C, lanes 2–4 and Figure 7D). This activity likely comes from DCP2 because the DCP1 trimerization mutant (Mut1), which does not interact with DCP2 and EDC4, does not copurify with decapping activity (Supplementary Figure S2E and F) (16).

Strikingly, the DCP1 GSSG mutant was strongly impaired (Figure 7C, lanes 5–7, and Figure 7D), although this mutant interacts with both DCP2 and EDC4 and coimmunoprecipitates with endogenous DCP2 and EDC4 (Figure 7A, B and E). The double mutations (R72G,N74G) also reduced decapping activity (Supplementary Figure S2E,F; mutant R,N), despite the ability of these mutants to interact with DCP2. As a control, we also tested mutations in DCP1 helix α1 that reduced DCP2 binding (S,Q,H). This mutant exhibited reduced decapping activity, as expected (Supplementary Figure S2E and F). We conclude that mutations in the NR-loop interfere with DCP2 activation by DCP1, without affecting the assembly of the DCP2–DCP1–EDC4 complex.

The docking of DCP1 and DCP2 on the EDC4 scaffold is crucial for decapping *in vivo*

Next, we investigated the functional relevance of the interfaces described in this study for decapping *in vivo*. To monitor mRNA decapping, we targeted a reporter mRNA for decapping-dependent degradation using a MS2-based tethering assay. MS2-tagged SMG7 protein was tethered to a β-globin reporter containing six MS2 binding sites in the 3′ UTR (β-globin-6MS2) (26). SMG7 is an effector protein in the nonsense-mediated mRNA decay pathway that directs bound mRNAs to the 5′-to-3′ decay pathway and thus causes deadenylation, followed by decapping and ultimately, 5′-to-3′ exonucleolytic degradation of the mRNA by XRN1 (27,34). Consequently, inhibiting decapping results in the accumulation of capped, deadenylated mRNA decay intermediates (because deadenylation precedes decapping), which can be detected on denaturing gels by their increased mobility (23,27).

Tethered MS2–SMG7 reduced β-globin-6MS2 mRNA levels relative to the MS2 protein alone (Figure 8A, lane 2 vs. 1, and Supplementary Figure S3A). The expression of the β-globin control mRNA lacking the MS2-binding sites was not affected (Figure 8A, lane 2 vs. 1; control). The overexpression of a catalytically inactive DCP2 mutant (E148Q) inhibited decapping in a dominant-negative manner, resulting in the accumulation of a deadenylated decay intermediate (Figure 8A, lane 6 vs. 5) (27). As a control, overexpression of wild type DCP2 had no effect (Figure 8A, lane 4). We confirmed that the change in mobility of the β-globin-6MS2 mRNA was caused by deadenylation using an oligo(dT)-directed ribonuclease H (RNase H) cleavage assay (Supplementary Figure S3B).

The overexpression of the DCP2 D15A,R19A mutant also inhibited decapping as efficiently as the overexpression of the catalytically inactive mutant (Figure 8A, lane 8, and Supplementary Figure S3A; D,R mutant), indicating that DCP2 activation by DCP1 is essential for decapping in human cells. Remarkably, the dominant negative effect of the D15A and R19A mutations was abolished when these mutations were combined with mutations in the FEB motif (Figures 8A, lane 10; D,R+3×F-A). The simplest explanation for this result is that the combined mutant does not interact with DCP1 and EDC4 and thus, cannot displace endogenous DCP2 from active decapping complexes. In contrast, the DCP2 D15A,R19A mutant competes with endogenous DCP2 for binding to EDC4 but fails to interact productively with

Figure 6. Continued
as in Figure 4D. The hinge region is shown in red. (**E**) A close up view of the hinge region observed in the closed conformation. (**F** and **G**) The interactions of GFP–DCP2 (wild type or mutants) with HA–EDC4 (F) and HA–DCP1a (G) were analyzed as described in Figure 1B. (**H**) A close up view of the catalytic site and the RNA binding groove. Selected residues are shown as sticks in cyan (DCP1) or green (DCP2). The residues mutated in this study are highlighted in purple (DCP1) and orange (DCP2) and labeled with a cyan and yellow backgrounds, respectively. Tryptophan W44 is shown in yellow and orange in the orientation observed in the open and closed Dcp2 conformations, respectively. The ATP molecule mimics the cap analog and was transferred from the *Sp* Dcp1–Dcp2 co-crystal structure to indicate the active site. Two nucleotides of RNA were modeled to indicate the putative binding path of the mRNA.

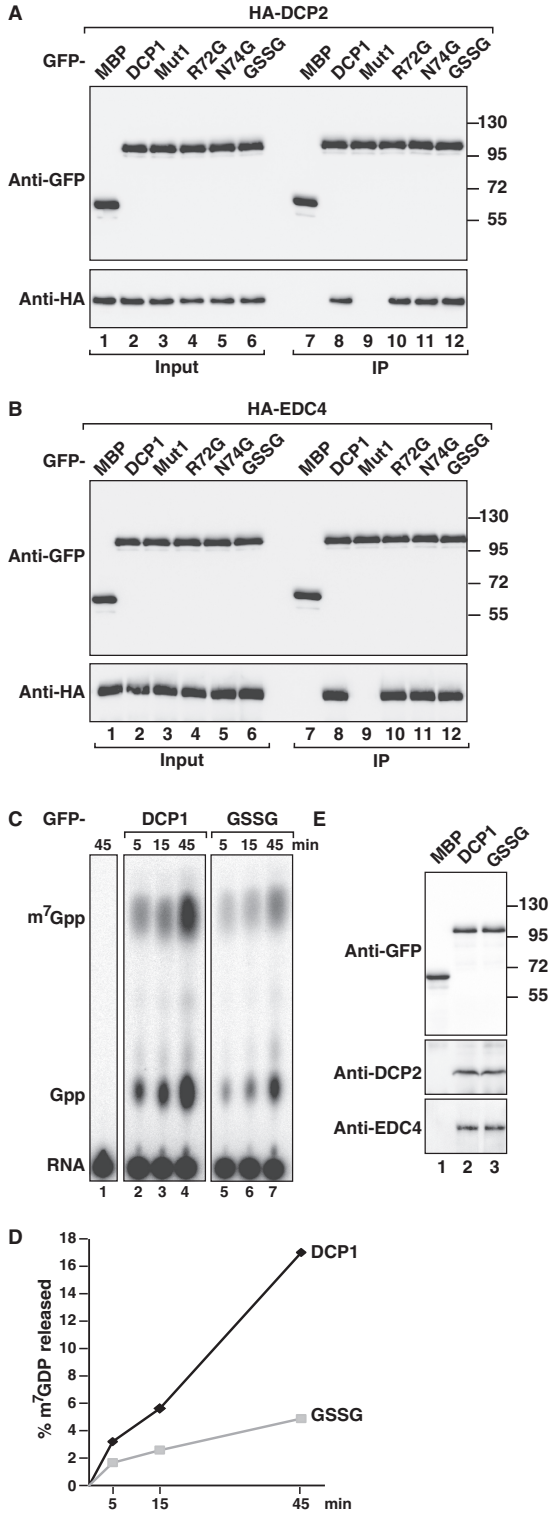

Figure 7. The DCP1 NR-loop plays a critical role in DCP2 activation. (**A** and **B**) The interaction of GFP–DCP1a (wild type or mutants) with HA–DCP2 (A) and HA–EDC4 (B). Inputs (1.5% and 1% for the GFP- and HA-tagged proteins, respectively) and bound fractions (IP; 30% and 20% for the GFP- and HA-tagged proteins, respectively) were analyzed by western blotting. (**C**,**D**) The GFP–DCP1 (wild type or the GSSG mutant) was expressed in HEK293T cells. The proteins were immunopurified using anti-GFP antibodies and tested for decapping activity *in vitro* as described in Figure 6A and B. (**E**) The samples corresponding to (C) were analyzed by western blotting using anti-GFP, anti-DCP2 and anti-EDC4 antibodies.

DCP1 and is therefore not activated, inhibiting decapping in a dominant negative manner.

Consistent with the above interpretation, the overexpression of the DCP2 C-terminal extension (residues 245–420), which is sufficient for EDC4 binding, also inhibited decapping and the degradation of the β-globin-6MS2 mRNA in a dominant manner, resulting in the accumulation of the deadenylated decay intermediate (Figure 8A, lane 14). Again, this effect was suppressed by mutations in the FEB motif (Figure 8A, lane 16). Thus, binding to EDC4 is required for the DCP2 mutants to exert a dominant negative effect. Accordingly, the dominant negative effect of the catalytically inert DCP2 mutant E148Q was abolished by mutations in the FEB motif (Figure 8B, lanes 8 vs. 6). The isolated FEB could not be tested because it was not stably expressed in human cells (Figure 1B). All proteins were expressed at comparable levels (Supplementary Figures S3C and D).

Finally, the G96P,V97P mutations in the hinge region and the W44A and K130A substitutions also inhibited decapping in a dominant negative manner (Figure 8B, lanes 10, 12, 14), consistent with the lack of catalytic activity *in vitro*, whereas a DCP2 fragment containing the NRD and the Nudix domain (1–244) was ineffective (Figure 8A, lane 12), most likely because it lacks the ability to bind EDC4.

To further validate our conclusions, we investigated the effects of the aforementioned mutants in decapping induced by the silencing domain of TNRC6A (6 A-SD), which is involved in the miRNA pathway and triggers deadenylation-dependent decapping (35,36). We observed that the DCP2 D15A,R19A mutant and the C-terminal extension inhibited decapping of the reporter as efficiently as the E148Q mutation (Figure 8C, lanes 6, 8 and 14). The inhibitory effect of these mutations was suppressed when they were combined with the 3×F-A mutations (Figure 8C, lanes 10 and 16).

We conclude that DCP2 mutants that bind EDC4 but are catalytically inert or fail to be activated by DCP1 inhibit decapping in a dominant negative manner independently of the mechanism by which the decapping complex is recruited to the mRNA target. The results also indicate that DCP2 binding to EDC4 is required for decapping *in vivo*.

Next, we tested for dominant negative effects of the GSSG substitution in the NR-loop of the DCP1 EVH1 domain, because this substitution exhibited the strongest inhibitory effect on DCP2 activity *in vitro* (Figure 7C and D). We observed that the DCP1 GSSG mutant inhibited decapping induced by SMG7 or TNRC6A-SD (Figure 8D and E, lane 6; Supplementary Figure 3F). Because this mutant binds both DCP2 and EDC4, it likely competes with endogenous DCP1 for incorporation into decapping complexes but fails to activate DCP2 in these complexes. These results indicate that the DCP1 NR-loop is required for DCP2-mediated decapping *in vivo*.

DISCUSSION

In this study, we show that EDC4 functions as a binding platform for DCP1, DCP2 and XRN1 and therefore

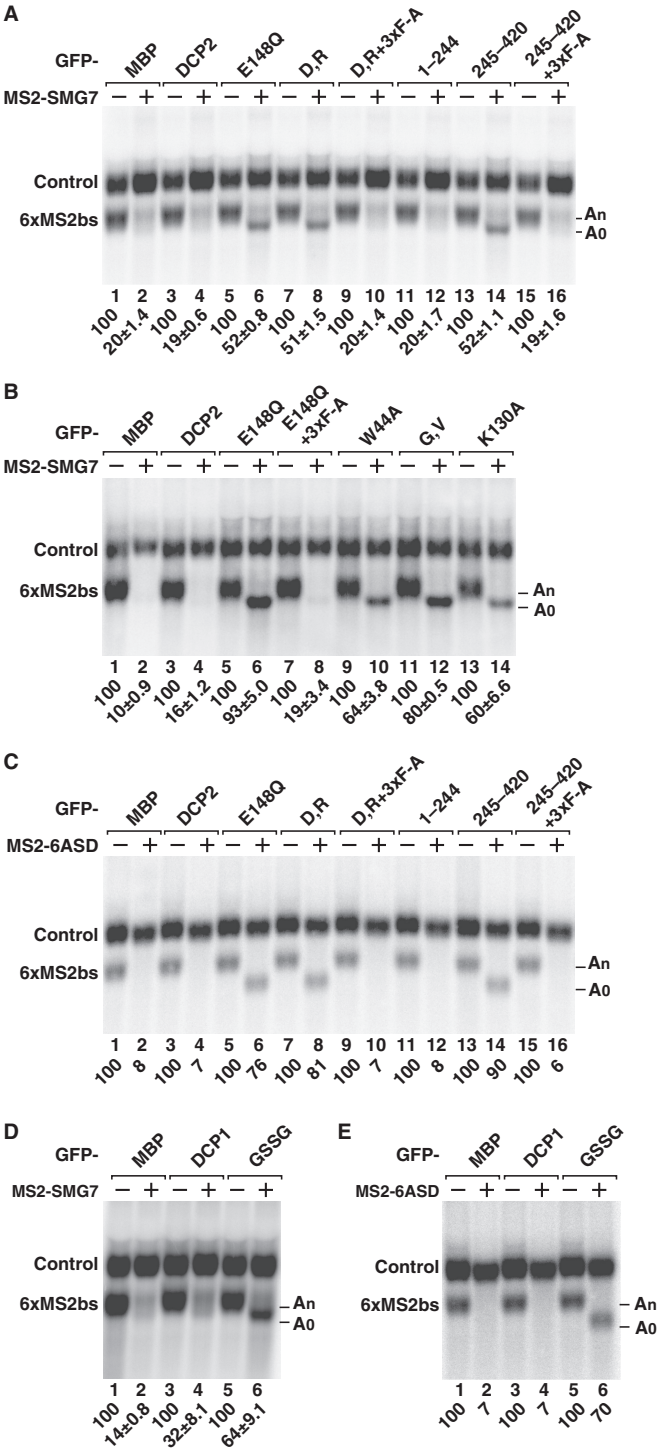

Figure 8. The DCP2 interaction with DCP1 and EDC4 is required for decapping *in vivo*. (**A** and **B**) Human HEK293T cells were transfected with a mixture of four plasmids: one expressing β-globin-6xMS2bs mRNA, another expressing MS2-HA or MS2–HA–SMG7, a third expressing a transfection control lacking the MS2 binding sites (control), and a fourth expressing GFP–MBP or GFP–DCP2 (wild type or the indicated mutants). (A) and (B) show northern blots of representative RNA samples. The positions of the polyadenylated (A_n) and deadenylated (A_0) β-globin-6xMS2bs reporter are indicated on the right. The β-globin-6xMS2bs mRNA levels were normalized to those of the control mRNA. These normalized values were set to 100 in cells expressing MS2-HA. The mean values ± standard deviations from three independent experiments are indicated below the panels and shown in Supplementary Figures S3A and E. The western blots demonstrating equivalent expression of the GFP-tagged proteins are shown in Supplementary Figures S3C and D. (**C**) A tethering assays using the β-globin-6xMS2bs reporter was performed as described above, with the exception that MS2–HA–SMG7 was replaced by MS2–HA–TNRC6A–SD. The numbers below the panel indicate the normalized β-globin-6xMS2bs mRNA levels. (**D** and **E**) Tethering assays using the β-globin-6xMS2bs reporter and MS2–SMG7 (D) or TNRC6A–SD (E) were performed as described in (A), with the exception that plasmids expressing GFP–DCP1 (wild type or GSSG mutant) were included in the transfection mixtures as indicated. The normalized values of the β-globin-6xMS2bs mRNA levels are indicated below the panels and shown in Supplemental Figure S3F. A western blot analysis demonstrating equivalent expression of the GFP-tagged proteins is shown in Supplementary Figure S3G.

orchestrates the assembly of the decapping complex and likely coordinates DCP2 activation with 5′-to-3′ degradation by XRN1 in human cells. Collectively, our results suggest a model for the assembly of the decapping complex wherein DCP1 and DCP2 dock on the EDC4 N- and C-terminal domains, respectively (Figure 9). These interactions bring the DCP1 EVH1 domain and the DCP2 NRD into close proximity so that they can directly interact. This interaction activates decapping by a mechanism that involves the NR-loop in the DCP1 EVH1 domain. The binding of XRN1 to the same EDC4 scaffold positions XRN1 at the location where decapped mRNAs are produced, thereby accelerating their degradation.

The assembly of the human decapping complex

The observation that EDC4 is required to bridge the DCP1 and DCP2 interaction in metazoan (15,24) has raised the question of whether the assembly of the decapping complex and the mechanism underlying DCP2 activation by DCP1 are conserved. Our results indicate that the DCP1 EVH1 domain and the DCP2 NRD interact in a similar manner as observed in the yeast complex (10). However, this interaction is weak, and an additional interaction bridged by EDC4 is required to strengthen the DCP1–DCP2 association. Thus, the DCP1–DCP2 interaction is likely to be favored when these molecules are bound to the same EDC4 scaffold *in vivo*. Consistent with this model, DCP2 mutants that are catalytically inert (e.g. E148Q) or that do not interact with DCP1 (e.g. D,R) inhibit decapping in a dominant negative manner only if they bind to EDC4, suggesting that binding to EDC4 is an obligatory step for decapping *in vivo*. Accordingly, EDC4 depletion inhibits decapping in human and *Drosophila melanogaster* cells (15,37). Whether EDC4 functions merely as a scaffold to bring DCP1 and DCP2 in close proximity or has a more direct role in promoting conformational changes in DCP2 remains unclear. The stabilization of the DCP1–DCP2 interaction by EDC4 may have allowed the DCP1–DCP2 interface to diverge, leading to a decrease in the affinity of DCP1 for DCP2 and consequently making EDC4 binding essential for the assembly of active decapping complexes.

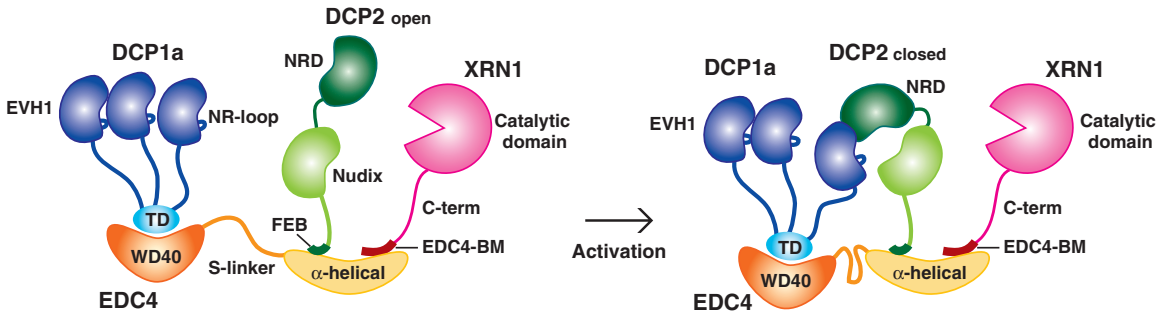

Figure 9. Model for the assembly of the human decapping complex. EDC4 provides binding sites for DCP1 trimers at its N-terminal WD40 domain and for DCP2 and XRN1 at its C-terminal α-helical domain. The DCP1 EVH1 domain can then interact with the DCP2 NRD and promote the active, closed DCP2 conformation by a mechanism that involves the NR-loop in the DCP1 EVH1 domain. The binding of XRN1 to the same EDC4 scaffold ensures that decapped mRNAs are transferred to XRN1. DCP1 trimerization is required for binding to EDC4 and DCP2, although it is not clear how. Furthermore EDC4 oligomerizes but the stoichiometry of the oligomers is unknown. Symbols are as described in Figure 1A.

The EDC4 binding motif in DCP2 (the FEB motif) is well conserved in vertebrates and appears to be also present in some invertebrate species and plants (Figure 1C). However, whether it mediates binding to EDC4 in these organisms needs to be tested experimentally. In contrast, the EDC4 binding motif (EDC4–BM) in XRN1 is restricted to vertebrates (Supplementary Figure S1A) (23). Nevertheless, an equivalent complex containing DCP1, DCP2, EDC4 and XRN1 assembles in insects wherein XRN1 interacts with DCP1 through a short proline-rich sequence (23). Thus, it is possible that a DCP1–DCP2–EDC4–XRN1 complex assembles in other metazoan species, although the individual interactions between orthologs might not be conserved. Indeed, some of the interactions in this complex are mediated by short linear motifs (e.g. FEB, EDC4–BM), which tend to evolve rapidly (38), rewiring the interaction network during evolution (3,38).

The conserved NR-loop in the DCP1 EVH1 domain plays a critical role in DCP2 activation

It has been proposed, but not tested, that residues in the DCP1 NR-loop play a role in DCP2 activation by inducing conformational changes in DCP2 residues that contact the substrate and position it for catalysis (10). Accordingly, substitutions of residues in the DCP1 NR-loop have been previously shown to cause decapping defects both *in vivo* and *in vitro* (10,11). However, because residues in the NR-loop also contact the DCP2 NRD, it has remained unclear whether they also contribute to the DCP1–DCP2 interaction.

In a study by She *et al.* (9), a sextuple *Sc* DCP1 mutant was generated with mutations in both the NR-loop and helix α1 of the EVH1 domain. These mutations disrupted DCP2 binding and decapping in yeast cells, but the specific contribution of the NR-loop to these effects was not investigated. On the other hand, a double alanine substitution of *Sc* Dcp1 residues R147 and D151 (corresponding to *Hs* DCP1 R71 and H76, respectively) was reported to not result in a decapping defect *in vivo* (39). In contrast, a substitution of loop residue P74 with serine (corresponding to human M75) conferred a temperature-sensitive phenotype in *S. pombe*, and yeast strains carrying the mutation were defective in mRNA decapping at the non-permissive temperature, although the interaction with DCP2 was not affected (11). Our results indicate that amino acid substitutions that render the NR-loop flexible do not prevent the interaction of DCP1 with DCP2 or its incorporation in decapping complexes but do interfere with DCP2 activation in a dominant manner.

How is the NR-loop involved in DCP2 activation? One possible model is that the NR-loop stabilizes the 'gatekeeper' W44 residue in the active conformation (10,14). Our study confirms an essential role for *Hs* DCP2 W44 in the catalytic mechanism. However, the NR-loop is more than 4 Å apart from *Sp* Dcp2 W43 in the co-crystal structure of the *Sp* Dcp1–Dcp2 complex (Figure 4E), and it is unclear whether it can contact this residue directly (14,33).

An alternative possibility is that the NR-loop is involved in the binding of the RNA substrate and/or the positioning of the RNA in the active site to allow the hydrolysis of the cap structure. Indeed, the NR-loop is located at the channel through which the RNA has been proposed to thread toward the active site (10), and it contains polar/hydrophilic residues that could bind the RNA backbone. The substitution of this well-defined loop with a flexible GSSG loop might obstruct the entrance to the RNA binding channel, explaining the inhibitory effect of this substitution.

In summary, we show that the basic DCP2 catalytic and activation mechanisms have been maintained throughout evolution. However, the acquisition of EDC4, the rapid evolution of protein-binding motifs in the C-terminal extensions of DCP2 and XRN1 and the presence of oligomerization domains in both DCP1 and EDC4 have increased the connectivity and complexity of the metazoan decapping complex (3), which in turn enhance opportunities for regulating the assembly and activity of the decapping complex and may enable coupling of decapping to 5′-to-3′ mRNA degradation. An important challenge for future studies is the elucidation of the stoichiometry of the human decapping complex and of the molecular basis for the interactions between its components.

SUPPLEMENTARY DATA

Supplementary Data are available at NAR Online.

ACKNOWLEDGEMENTS

We are grateful to L. Gasse for generating the DCP1 GSSG mutant, C. Igreja, D. Kuzuoğlu-Öztürk and L. Zekri for insightful comments on the manuscript and S. Helms and C. Weiler for technical assistance.

FUNDING

The Max Planck Society; the Deutsche Forschungsgemeinschaft [DFG, FOR855 and the Gottfried Wilhelm Leibniz Program awarded to E.I.]; the European Union Seventh Framework Programme through a Marie Curie Fellowship [FP7, 275343 to S.J.]. Funding for open access charge: Max Planck Society.

Conflict of interest statement. None declared.

REFERENCES

1. Arribas-Layton,M., Wu,D., Lykke-Andersen,J. and Song,H. (2013) Structural and functional control of the eukaryotic mRNA decapping machinery. *Biochim. Biophys. Acta*, **1829**, 580–589.
2. Ling,S.H., Qamra,R. and Song,H. (2011) Structural and functional insights into eukaryotic mRNA decapping. *Wiley Interdiscip Rev. RNA*, **2**, 193–208.
3. Jonas,S. and Izaurralde,E. (2013) The role of disordered protein regions in the assembly of decapping complexes and RNP granules. *Genes Dev.*, **27**, 2628–2641.
4. Lykke-Andersen,J. (2002) Identification of a human decapping complex associated with hUpf proteins in nonsense-mediated decay. *Mol. Cell. Biol.*, **22**, 8114–8121.
5. van Dijk,E., Cougot,N., Meyer,S., Babajko,S., Wahle,E. and Seraphin,B. (2002) Human Dcp2: a catalytically active mRNA decapping enzyme located in specific cytoplasmic structures. *EMBO J.*, **21**, 6915–6924.
6. Wang,Z., Jiao,X., Carr-Schmid,A. and Kiledjian,M. (2002) The hDcp2 protein is a mammalian mRNA decapping enzyme. *Proc. Natl Acad. Sci. USA*, **99**, 12663–12668.
7. Steiger,M., Carr-Schmid,A., Schwartz,D.C., Kiledjian,M. and Parker,R. (2003) Analysis of recombinant yeast decapping enzyme. *RNA*, **9**, 231–238.
8. Dunckley,T. and Parker,R. (1999) The DCP2 protein is required for mRNA decapping in *Saccharomyces cerevisiae* and contains a functional MutT motif. *EMBO J.*, **18**, 5411–5422.
9. She,M., Decker,C.J., Chen,N., Tumati,S., Parker,R. and Song,H. (2006) Crystal structure and functional analysis of Dcp2p from *Schizosaccharomyces pombe*. *Nat. Struct. Mol. Biol.*, **13**, 63–70.
10. She,M., Decker,C.J., Svergun,D.I., Round,A., Chen,N., Muhlrad,D., Parker,R. and Song,H. (2008) Structural basis of dcp2 recognition and activation by dcp1. *Mol. Cell*, **29**, 337–349.
11. Sakuno,T., Araki,Y., Ohya,Y., Kofuji,S., Takahashi,S., Hoshino,S. and Katada,T. (2004) Decapping reaction of mRNA requires Dcp1 in fission yeast: its characterization in different species from yeast to human. *J. Biochem.*, **136**, 805–812.
12. Deshmukh,M.V., Jones,B.N., Quang-Dang,D.U., Flinders,J., Floor,S.N., Kim,C., Jemielity,J., Kalek,M., Darzynkiewicz,E. and Gross,J.D. (2008) mRNA decapping is promoted by an RNA-binding channel in Dcp2. *Mol. Cell*, **29**, 324–336.
13. Floor,S.N., Jones,B.N., Hernandez,G.A. and Gross,J.D. (2010) A split active site couples cap recognition by Dcp2 to activation. *Nat. Struct. Mol. Biol.*, **17**, 1096–1101.
14. Floor,S.N., Borja,M.S. and Gross,J.D. (2012) Interdomain dynamics and coactivation of the mRNA decapping enzyme Dcp2 are mediated by a gatekeeper tryptophan. *Proc. Natl Acad. Sci. USA*, **109**, 2872–2877.
15. Fenger-Grøn,M., Fillman,C., Norrild,B. and Lykke-Andersen,J. (2005) Multiple processing body factors and the ARE binding protein TTP activate mRNA decapping. *Mol. Cell*, **20**, 905–915.
16. Tritschler,F., Braun,J.E., Motz,C., Igreja,C., Haas,G., Truffault,V., Izaurralde,E. and Weichenrieder,O. (2009) DCP1 forms asymmetric trimers to assemble into active mRNA decapping complexes in metazoa. *Proc. Natl Acad. Sci. USA*, **106**, 21591–21596.
17. Bloch,D.B., Nobre,R.A., Bernstein,G.A. and Yang,W.H. (2011) Identification and characterization of protein interactions in the mammalian mRNA processing body using a novel two-hybrid assay. *Exp. Cell Res.*, **317**, 2183–2199.
18. Decker,C.J. and Parker,R. (1993) A turnover pathway for both stable and unstable mRNAs in yeast: evidence for a requirement for deadenylation. *Genes Dev.*, **7**, 1632–1643.
19. Hsu,C.L. and Stevens,A. (1993) Yeast cells lacking 5′→3′ exoribonuclease 1 contain mRNA species that are poly(A) deficient and partially lack the 5′ cap structure. *Mol. Cell. Biol.*, **13**, 4826–4835.
20. Muhlrad,D., Decker,C.J. and Parker,R. (1994) Deadenylation of the unstable mRNA encoded by the yeast MFA2 gene leads to decapping followed by 5′→3′ digestion of the transcript. *Genes Dev.*, **8**, 855–866.
21. Chang,J.H., Xiang,S., Xiang,K., Manley,J.L. and Tong,L. (2011) Structural and biochemical studies of the 5′→3′ exoribonuclease Xrn1. *Nat. Struct. Mol. Biol.*, **18**, 270–276.
22. Jínek,M., Coyle,S.M. and Doudna,J.A. (2011) Coupled 5′ nucleotide recognition and processivity in Xrn1-mediated mRNA decay. *Mol. Cell*, **41**, 600–608.
23. Braun,J.E., Truffault,V., Boland,A., Huntzinger,E., Chang,C.T., Haas,G., Weichenrieder,O., Coles,M. and Izaurralde,E. (2012) A direct interaction between DCP1 and XRN1 couples mRNA decapping to 5′ exonucleolytic degradation. *Nat. Struct. Mol. Biol.*, **19**, 1324–1331.
24. Xu,J., Yang,J.Y., Niu,Q.W. and Chua,N.H. (2006) Arabidopsis DCP2, DCP1, and VARICOSE Form a Decapping complex required for postembryonic development. *Plant Cell*, **18**, 3386–3398.
25. Jínek,M., Eulalio,A., Lingel,A., Helms,S., Conti,E. and Izaurralde,E. (2008) The C-terminal region of Ge-1 presents conserved structural features required for P-body localization. *RNA*, **14**, 1991–1998.
26. Lykke-Andersen,J., Shu,M.D. and Steitz,J.A. (2000) Human Upf proteins target an mRNA for nonsense-mediated decay when bound downstream of a termination codon. *Cell*, **103**, 1121–1131.
27. Loh,B., Jonas,S. and Izaurralde,E. (2013) The SMG5-SMG7 heterodimer directly recruits the CCR4-NOT deadenylase complex to mRNAs containing nonsense codons via interaction with POP2. *Genes Dev.*, **27**, 2125–2138.
28. Diebold,M.L., Fribourg,S., Koch,M., Metzger,T. and Romier,C. (2011) Deciphering correct strategies for multiprotein complex assembly by co-expression: application to complexes as large as the histone octamer. *J. Struct. Biol.*, **175**, 178–188.
29. Kelley,L.A. and Sternberg,M.J.E. (2009) Protein structure prediction on the web: a case study using the Phyre server. *Nat. Protocols*, **4**, 363–371.
30. Studier,W.F. (2005) Protein production by auto-induction in high-density shaking cultures. *Prot. Exp. Pur.*, **1**, 207–234.
31. Lai,T., Cho,H., Liu,Z., Bowler,M.W., Piao,S., Parker,R., Kim,Y.K. and Song,H. (2012) Structural basis of the PNRC2-mediated link between mRNA surveillance and decapping. *Structure*, **20**, 2025–2037.
32. Yu,J.H., Yang,W.H., Gulick,T., Bloch,K.D. and Bloch,D.B. (2005) Ge-1 is a central component of the mammalian cytoplasmic mRNA processing body. *RNA*, **11**, 1795–1802.
33. Aglietti,R.A., Floor,S.N., McClendon,C.L., Jacobson,M.P. and Gross,J.D. (2013) Active site conformational dynamics are coupled to catalysis in the mRNA decapping enzyme dcp2. *Structure*, **21**, 1571–1580.

34. Unterholzner,L. and Izaurralde,E. (2004) SMG7 acts as a molecular link between mRNA surveillance and mRNA decay. *Mol. Cell*, **16**, 587–596.
35. Braun,J.E., Huntzinger,E., Fauser,M. and Izaurralde,E. (2011) GW182 proteins directly recruit cytoplasmic deadenylase complexes to miRNA targets. *Mol. Cell*, **44**, 120–133.
36. Fabian,M.R. and Sonenberg,N. (2012) The mechanics of miRNA-mediated gene silencing: a look under the hood of miRISC. *Nat. Struct. Mol. Biol.*, **19**, 586–593.
37. Eulalio,A., Rehwinkel,J., Stricker,M., Huntzinger,E., Yang,S.F., Doerks,T., Dorner,S., Bork,P., Boutros,M. and Izaurralde,E. (2007) Target-specific requirements for enhancers of decapping in miRNA-mediated gene silencing. *Genes Dev.*, **21**, 2558–2570.
38. Davey,N.E., Van Roey,K., Weatheritt,R.J., Toedt,G., Uyar,B., Altenberg,B., Budd,A., Diella,F., Dinkel,H. and Gibson,T.J. (2012) Attributes of short linear motifs. *Mol. Biosyst.*, **8**, 268–281.
39. Tharun,S. and Parker,R. (1999) Analysis of Muations of the yeast mRNA decapping enzyme. *Genetics*, **151**, 1273–1285.